

Orbital magnetization and its effects in spin-chiral ferromagnetic kagomé lattice in the general spin-coupling region

Zhigang Wang and Ping Zhang

Institute of Applied Physics and Computational Mathematics, P.O. Box 8009, Beijing 100088, P.R. China

The orbital magnetization and its effects on the two-dimensional kagomé lattice with spin anisotropies included in the general Hund's coupling region have been theoretically studied. The results show that the strength of the Hund's coupling, as well as the spin chirality, contributes to the orbital magnetization \mathcal{M} . Upon varying both these parameters, it is found that the two parts of \mathcal{M} , i.e., the conventional part \mathbf{M}_c and the Berry-phase correction part \mathbf{M}_Ω , oppose each other. The anomalous Nernst conductivity is also calculated and a peak-valley structure as a function of the electron Fermi energy is obtained.

PACS numbers: 75.30.-m, 73.43.-f, 72.15.Jf

I. INTRODUCTION

Recently the geometrically frustrated electron systems have provided hot topics in the field of condensed matter physics [1]. Ferromagnetic pyrochlore $R_2\text{Mo}_2\text{O}_7$ ($R=\text{Nd}, \text{Sm}, \text{Gd}$) is one key type of the geometrically frustrated systems [2], which consists of corner-sharing tetrahedrons and the antiferromagnetic interactions between nearest-neighbor spins are frustrated. It was recently pointed out that even the ferromagnetic interaction is frustrated, if the spin easy axis points to the center of the tetrahedron [3]. In this case, the spin chirality [4], which originated from the noncoplanar spin configuration, is expected to affect the quantum of the electrons, especially the transverse conductivity. This mechanism is also called "Berry phase contribution" because a non-vanishing spin chirality is associated with a non-vanishing spin Berry phase for conduction electrons. To interpret the transport experiments on ferromagnetic pyrochlore [5, 6], Ohgushi et al. [7] studied the Hall effect in a two-dimensional (2D) kagomé lattice, which is the cross section of the pyrochlore lattice perpendicular to the (1,1,1) direction [2]. They obtained that if the chiral spin state is realized, the system can show a quantized Hall effect. In their model an important limit is used, which is that the electron conduction spins are colinear with lattice (ions) spins. This limit is called that "the strong (or infinite) Hund's coupling limit". However, detailed experiments on the pyrochlores [8] show that the chiral mechanism alone can not explain the anomalous transport phenomena in these systems. To explain these experiments, Taillefumier et al. [9] studied the same lattice in a general case, which extrapolates the strong and weak Hund's coupling regions. They found that the spin Berry phase contribution does not depend only on the spin chirality, but also on the strength of the local Hund's coupling.

On the other hand, the orbital magnetism of Bloch electrons has been attracted renewed interest, due to the recent recognition [10, 11, 12] that the Berry phase effect plays an important role on orbital magnetism as well as on the Hall conductivity. The Berry phase effect on orbital magnetism was until now partially presented by

very few studies [12, 13, 14, 15, 16]. Due to its basic importance in understanding the magnetism and transport features of the materials, obviously, more work are needed in exploiting the Berry phase effect on the properties of the orbital magnetization (OM) in various kinds of realistic physical systems.

In this paper we extend the study of the OM to the ferromagnetic pyrochlore systems; more specially, we focus our attention to the 2D kagomé lattice with spin anisotropies and Hund's coupling included. It is found that the two parts in OM (see Sec. II), i.e., the conventional part M_c and the Berry-phase correction part M_Ω , oppose each other. In particular, the OM displays fully different behaviors in metallic and insulating regions due to the different roles M_c and M_Ω play in these two regions. Moreover, similar to the role the Hund's coupling plays in determining the anomalous Hall conductivity as observed in the above-mentioned experimental [8] and theoretical [9] works, we find that the OM is also importantly affected by the Hund's coupling. In particular, in the weak coupling case that the Mott gap between the upper and lower Hubbard bands is overcome by the electron kinetic energy, we show that the OM exhibits complex behaviors when scanning the Fermi energy through the whole series of occupied bands. Furthermore, by using the obtained values of the OM we also calculate the anomalous Nernst conductivity, which is featured by a complicated peak-valley pattern as a function of the electron Fermi energy.

II. PRELIMINARIES

Before studying the OM of the 2D kagomé lattice, we simply review the general multiband formula for finite-temperature OM in the semiclassical picture of Bloch electrons. In the semiclassical picture [17, 18], the Bloch electron for the n th band is treated as a wave packet $|w_n(\mathbf{r}_c, \mathbf{k}_c)\rangle$ with its center $(\mathbf{r}_c, \mathbf{k}_c)$ in the phase space. The orbital magnetic moment characterizes the rotation of the wave packet around its centroid and is given by $\mathbf{m}_n(\mathbf{k}_c) = \frac{-e}{2} \langle w_n | (\hat{\mathbf{r}} - \mathbf{r}_c) \times \hat{\mathbf{v}} | w_n \rangle$, where $(-e)$ is the

charge of the electron and $\hat{\mathbf{v}}$ is the velocity operator. By writing the wave packet in terms of the Bloch state, one obtains (\mathbf{k}_c is abbreviated as \mathbf{k})

$$\mathbf{m}_n(\mathbf{k}) = -i(e/2\hbar)\langle \nabla_{\mathbf{k}} u_{n\mathbf{k}} | \times [\hat{H}_{\mathbf{k}} - \varepsilon_{n\mathbf{k}}^{(0)}] | \nabla_{\mathbf{k}} u_{n\mathbf{k}} \rangle, \quad (1)$$

where $|u_{n\mathbf{k}}\rangle$ is the periodic part of the Bloch state with band energy $\varepsilon_{n\mathbf{k}}^{(0)}$, and $\hat{H}_{\mathbf{k}}$ is the crystal Hamiltonian acting on $|u_{n\mathbf{k}}\rangle$. However, it was further found [10] that the presence of a weak magnetic field \mathbf{B} will result in a modification of the density of states in the semi-classical phase space, $d^3\mathbf{k} \rightarrow d^3\mathbf{k}(1 + e\mathbf{B}\cdot\boldsymbol{\Omega}_n/\hbar)$, where $\boldsymbol{\Omega}_n(\mathbf{k}) = i\langle \nabla_{\mathbf{k}} u_{n\mathbf{k}} | \times | \nabla_{\mathbf{k}} u_{n\mathbf{k}} \rangle$ is the Berry curvature in k -space. Due to this weak-field modification and the additional thermodynamic average over Bloch bands included at finite temperature, the total free energy for an equilibrium ensemble of electrons in the weak field may be written as [10]

$$F = -\frac{1}{\beta} \sum_n \int d^3\mathbf{k} \left(1 + \frac{e}{\hbar} \mathbf{B} \cdot \boldsymbol{\Omega}_n(\mathbf{k}) \right) \ln[1 + e^{\beta(\mu - \varepsilon_{n\mathbf{k}})}]. \quad (2)$$

where μ is the electron chemical potential, $\beta = 1/k_B T$ and $\varepsilon_{n\mathbf{k}} = \varepsilon_{n\mathbf{k}}^{(0)} - \mathbf{m}_n(\mathbf{k}) \cdot \mathbf{B}$ is the electron band energy in the presence of the external magnetic field. The equilibrium OM density is given by the field derivative at fixed temperature and chemical potential, $\vec{\mathcal{M}} = -(\partial F / \partial \mathbf{B})_{\mu, T}$, with the result

$$\begin{aligned} \vec{\mathcal{M}} &= \sum_n \int d^3\mathbf{k} \mathbf{m}_n(\mathbf{k}) f_n \\ &+ \frac{1}{\beta} \sum_n \int d^3\mathbf{k} \frac{e}{\hbar} \boldsymbol{\Omega}_n(\mathbf{k}) \ln \left[1 + e^{\beta(\mu - \varepsilon_{n\mathbf{k}})} \right] \\ &\equiv \mathbf{M}_c + \mathbf{M}_{\Omega}, \end{aligned} \quad (3)$$

where f_n is the local equilibrium Fermi function for n th band. In addition to the conventional term \mathbf{M}_c in terms of the orbital magnetic moment $\mathbf{m}_n(\mathbf{k})$, the extra term \mathbf{M}_{Ω} in Eq. (3) is a Berry phase effect and exposes a new topological ingredient to the orbital magnetism. Interestingly, it is this Berry phase correction that eventually enters the thermal transport current [12]. At zero temperature and magnetic field the general expression (3) is reduced to [10]

$$\vec{\mathcal{M}} = \sum_n \int^{\mu_0} d^3\mathbf{k} \left(\mathbf{m}_n(\mathbf{k}) + \frac{e}{\hbar} \boldsymbol{\Omega}_n(\mathbf{k}) [\mu_0 - \varepsilon_{n\mathbf{k}}] \right), \quad (4)$$

where the upper limit means that the integral is over states with energies below the zero-temperature chemical

potential (Fermi energy) μ_0 .

III. THEORETICAL MODEL AND CHERN NUMBER

Following previous works [7, 9, 15], we consider the double-exchange ferromagnet kagomé lattice schematically shown in Fig. 1(a). The triangle is the one face of the tetrahedron. Here we consider a pure spin model with anisotropic Dzyaloshinskii-Moriya interactions on a kagomé lattice. It consists of an umbrella of three spins per unit cell of the kagomé lattice. Each umbrella can be described by the spherical coordinates of the three spins $(\pi/6, \theta)$, $(5\pi/6, \theta)$, and $(-\pi/2, \theta)$, as shown in Fig. 1(b). The angle θ ranges from 0 to π .

The tight-binding model of this 2D kagomé lattice can be written as the following [9]

$$H = \sum_{\langle i, j \rangle, \sigma} t_{ij} \left(c_{i\sigma}^\dagger c_{j\sigma} + \text{H.c.} \right) - J_0 \sum_{i, \alpha, \beta} c_{i\alpha}^\dagger (\boldsymbol{\sigma}_{\alpha\beta} \cdot \mathbf{n}_i) c_{i\beta}, \quad (5)$$

where t_{ij} is the hopping integral between two neighboring sites i and j ; $c_{i\sigma}^\dagger$ and $c_{i\sigma}$ are the creation and annihilation operators of an electron with spin σ on the site i . J_0 is the effective coupling constant to each local moment \mathbf{S}_i , and these moments are treated below as classical variables. \mathbf{n}_i is a unit vector collinear with the local moment \mathbf{S}_i . σ are the Pauli matrices. In the following we change notation $i \rightarrow (lm, s)$, where (lm) labels the kagomé unit cell and s is the site index in one unit cell. Note that in the infinite Hund's coupling limit, i.e., $J_0 \rightarrow \infty$, this system has already been discussed in Refs. [7, 15, 19]. In this limit the two $\sigma = \uparrow, \downarrow$ bands are infinitely split and the model describes a fully polarized electron subject to a modulation of a fictitious magnetic flux.

To diagonalize the Hamiltonian (5), we need to rewrite it in the reciprocal space. We use the momentum representation of the electron operator

$$c_{(lm, s, \sigma)} = \frac{1}{\sqrt{L_x L_y}} \sum_{\mathbf{k}} e^{i\mathbf{k} \cdot \mathbf{R}_{(lm, s)}} \gamma_{s\sigma}(\mathbf{k}) \quad (6)$$

and the one-particle state $|\Psi(\mathbf{k})\rangle = \sum_{s\sigma} \Psi_{s\sigma}(\mathbf{k}) \gamma_{s\sigma}^\dagger(\mathbf{k}) |0\rangle$. Inserting $|\Psi(\mathbf{k})\rangle$ into the Schrödinger equation $H|\Psi\rangle = E|\Psi\rangle$, we can easily obtain the Hamiltonian in the reciprocal space $H(\mathbf{k})$, which is given by

$$H(\mathbf{k}) = \begin{pmatrix} -J_0 \cos \theta & p_{\mathbf{k}}^1 & p_{\mathbf{k}}^3 & iJ_0 \sin \theta & 0 & 0 \\ p_{\mathbf{k}}^1 & -J_0 \cos \theta & p_{\mathbf{k}}^2 & 0 & -J_0 \sin \theta e^{-i\frac{\pi}{6}} & 0 \\ p_{\mathbf{k}}^3 & p_{\mathbf{k}}^2 & -J_0 \cos \theta & 0 & 0 & -J_0 \sin \theta e^{-i\frac{5\pi}{6}} \\ -iJ_0 \sin \theta & 0 & 0 & J_0 \cos \theta & p_{\mathbf{k}}^1 & p_{\mathbf{k}}^3 \\ 0 & -J_0 \sin \theta e^{i\frac{\pi}{6}} & 0 & p_{\mathbf{k}}^1 & J_0 \cos \theta & p_{\mathbf{k}}^2 \\ 0 & 0 & -J_0 \sin \theta e^{i\frac{5\pi}{6}} & p_{\mathbf{k}}^3 & p_{\mathbf{k}}^2 & J_0 \cos \theta \end{pmatrix}, \quad (7)$$

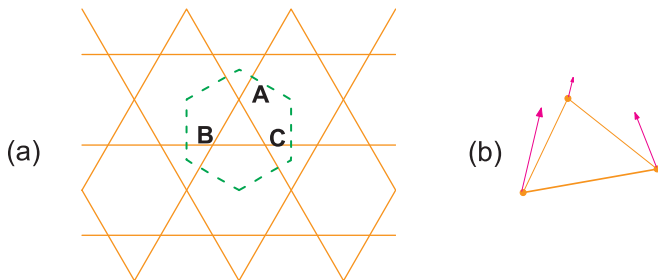


FIG. 1: (Color online) (a) Two dimensional spin-chiral ferromagnetic kagomé lattice. The dashed line represents the Wigner-Seitz unit cell, which contains three independent sites (A, B, C). (b) The umbrella structure on the triangular cell of the 2D kagomé lattice.

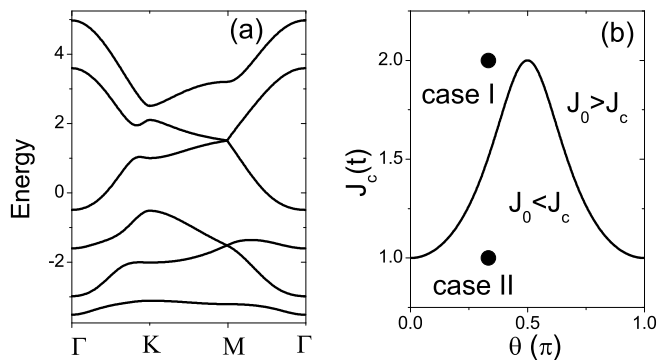


FIG. 2: (a) Energy spectrum of the 2D kagomé lattice with the parameters as $\theta = \pi/3$, $J_0 = J_c = 4/\sqrt{7}$. (b) The critical value of Hund's coupling J_c as a function of the chiral parameter θ .

where $t = |t_{ij}|$ as the energy unit and $p_{\mathbf{k}}^i = 2t \cos(\mathbf{k} \cdot \mathbf{a}_i)$. $\mathbf{a}_1 = (-\frac{1}{2}, -\frac{\sqrt{3}}{2})$, $\mathbf{a}_2 = (1, 0)$, and $\mathbf{a}_3 = (-\frac{1}{2}, \frac{\sqrt{3}}{2})$ represent the displacements in a unit cell from A to B site, from B to C site, and from C to A site respectively. In this notation, the Brillouin zone (BZ) is a hexagon with the corners of $\mathbf{k} = \pm(2\pi/3)\mathbf{a}_1$, $\pm(2\pi/3)\mathbf{a}_2$, $\pm(2\pi/3)\mathbf{a}_3$, two of which are independent.

Now let us consider the Chern number [20] and Hall conductivity of this system, which have been reported in Refs. [9, 21]. In the strong Hund's coupling limit, there

is an energy gap between the two nearest-neighbor bands in the cases of $\theta \neq 0, \pi$. Then the Hall conductivity is a sum over occupied Bloch bands,

$$\sigma_{xy} = \frac{e^2}{h} \sum_n^{\text{occu.}} C_n, \quad (8)$$

where the n th band Chern number is defined by

$$C_n = -\frac{1}{2\pi} \int_{\text{BZ}} d^2\mathbf{k} \Omega_n(\mathbf{k}) = -\frac{1}{2\pi} \int_{\text{BZ}} d^2\mathbf{k} \hat{z} \cdot [\nabla_{\mathbf{k}} \times \mathbf{A}_n(\mathbf{k})], \quad (9)$$

where $\mathbf{A}_n(\mathbf{k}) = i\langle u_{n\mathbf{k}} | \nabla_{\mathbf{k}} u_{n\mathbf{k}} \rangle$ is the Berry-phase connection (vector potential) for the n th band. At finite temperature, considering the electron density distribution, the Hall conductivity is written as

$$\sigma_{xy} = -\frac{e^2}{h} \int_{\text{BZ}} \frac{d^2\mathbf{k}}{2\pi} f_n \hat{z} \cdot [\nabla_{\mathbf{k}} \times \mathbf{A}_n(\mathbf{k})]. \quad (10)$$

However in the general spin coupling cases, the gap between two nearest-neighbor bands may disappear. When the Fermi energy lies in these two bands, because the gap vanishes, the Hall conductivity can not be written in the form of Eq. (8). In despite of this, the concept of the n th band Chern number and Eq. (8) are also useful when the gap between two nearest-neighbor bands does not disappear.

For the general cases the energy spectrum can only be computed numerically, except for general θ at high-symmetry points. For the finite values of J_0 , as pointed in [9], the splitting of the spectrum depends on two mechanisms. One is that the coupling J_0 separates each group of three bands, the other is that when switching on J_0 , the pointlike degeneracies are lifted within each group of three bands. According to the properties of the M point of the Brillouin zone, a critical value of the Hund's coupling as a function of the chiral parameter θ can be analytically obtained, which is given by [9],

$$J_c(\theta) = \pm \frac{2t}{\sqrt{1 + 3\cos^2\theta}}. \quad (11)$$

Using Eq. (11) one can distinguish between two different regimes depending on the value of J_0 as compared to $J_c(\theta)$. In the regime where $J_0 > J_c$, the Chern numbers associated with each band are given by $-1, 0, 1, 1, 0, -1$ from the lowest to the topmost band. Whereas in

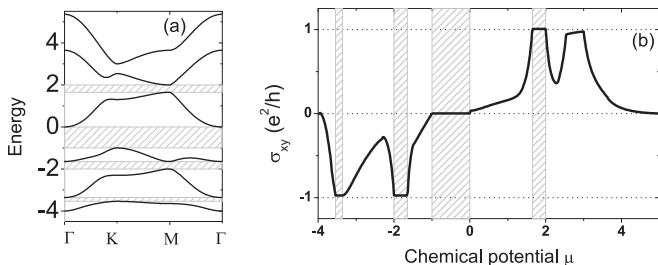


FIG. 3: (a) The energy spectrum of the 2D kagomé lattice. (b) The Hall conductivity σ_{xy} as a function of the chemical potential μ . In both figures, the chiral parameter is $\theta=\pi/3$ and the strength of the Hund's coupling $J_0=2$. The shaded areas are the energy gaps, which are labeled as gap-I, -II, -III, and -IV from the lowest to the topmost gap.

the regime where $J_0 < J_c$, the Chern numbers associated with each band are given by $-1, 3, -2, -2, 3, -1$ in the same order. We draw in Fig. 2(a) the energy spectrum with the spin chiral parameter $\theta=\pi/3$ and J_0 taking the critical value $J_c=4/\sqrt{7}$. Fig. 2(b) shows the critical value of the Hund's coupling J_c as a function of the chirality θ .

IV. THE ORBITAL MAGNETIZATION

Now we turn to study the OM of the 2D kagomé lattice in the general Hund's coupling cases. Similar to the Hall conductivity, the OM displays different behaviors in two regions which we will exhibit in turn. As examples, we consider two cases. The case I, in which we set the parameters as $\theta=\pi/3$ and $J_0=2$, is one typical case in the regime where $J_0 > J_c(=4/\sqrt{7} \approx 1.51)$. Whereas the case II, in which the parameters are $\theta=\pi/3$ and $J_0=1$, is another typical case in the regime where $J_0 < J_c$. These two cases are shown in Fig. 2(b) with solid dots.

First we consider the case I. To more clearly investigate the OM of the 2D kagomé lattice, we need to know the energy band structure of the system. So, we draw the energy spectrum in Fig. 3(a), from which one can find that there are four gaps. From the lowest to the topmost gap, we denote these gaps as gap-I, -II, -III, and -IV. Clearly, in this case only the gap between bands 5 and 6 vanishes. Fig. 3(b) plots the Hall conductivity as a function of the electron Fermi energy (chemical potential).

Figure 4(a) shows the OM (\mathcal{M}) as a function of the electron chemical potential μ . One can see that initially the OM rapidly decreases as the filling of the lowest band increases, arriving at a minimum at $\mu=-3.54$, a value corresponding to the top of the lowest band. Then, as the chemical potential continues to vary in the gap-I, the OM goes up and increases as a linear function of μ . This linear relationship in the insulating region can be

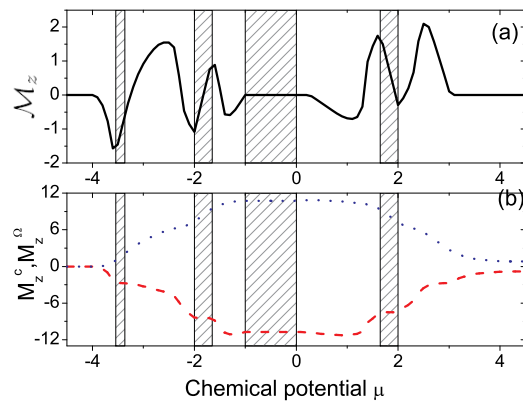


FIG. 4: (Color online) (a) The OM and (b) its two components M_c (dashed line) and M_Ω (dotted line) as a function of the chemical potential μ . The parameters are same as those in Fig. 3.

understood by Eq. (3), from which one obtains

$$\begin{aligned} \frac{d\mathcal{M}}{d\mu} &= \frac{e}{\hbar} \sum_n^{\text{occu}} \int d^2\mathbf{k} \Omega_n(\mathbf{k}) \\ &= -\frac{e}{\hbar} \sum_n^{\text{occu}} C_n. \end{aligned} \quad (12)$$

Thus when the chemical potential varies in the gap-I, only the lowest band is occupied and $d\mathcal{M}/d\mu = -(e/\hbar)C_1$. In this case, $C_1 = -1$. Thus $d\mathcal{M}/d\mu = e/\hbar$, i.e., the OM linearly increases with the chemical potential in the insulating region I, as shown in Fig. 4(a). Similarly, when the chemical potential increases in the gap-II, the OM increases linearly with μ . Since the Chern number of band 2 is zero, thus from Eq. (12) and Fig. 4(a) one can see that the slope of the OM curve in the gap-II is same as that in the gap-I. When the chemical potential increases in the gap-III, the OM becomes zero and does not vary with the chemical potential. The reason is that the sum over the Chern numbers of the occupied lowest three bands is zero. From Eq. (12), one can see that the slope of the OM is independent of μ . In fact the gap-III is the usually called the Mott gap. With the chemical potential increases, when it lies in the gap-IV, one can find that the OM decreases linearly with μ . The reason is that the sum of the Chern numbers of the lowest four bands is 1. From Eq. (12), one can find $d\mathcal{M}/d\mu = -e/\hbar$, i.e., the OM linearly decreases with the chemical potential in the gap-IV as shown in Fig. 3(b).

For further study, we show in Fig. 4(b) M_c and M_Ω as a function of the chemical potential, their sum gives \mathcal{M} in Fig. 4(a). One can see that overall M_c and M_Ω have opposite contributions to \mathcal{M} , which implies that these two parts carry opposite-circulating currents. In each insulating area the conventional term M_c keeps a constant, which is due to the fact that the upper limit of the k -integral of $m_n(\mathbf{k})$ is invariant as the chemical po-

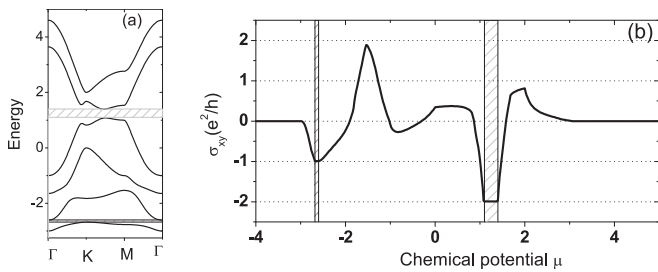


FIG. 5: (a) The energy spectrum of the 2D kagomé lattice. (b) The Hall conductivity σ_{xy} as a function of the chemical potential μ . In both figures, the chiral parameter is $\theta=\pi/3$ and the strength of the Hund's coupling $J_0=1$. The shaded areas are the energy gaps, which are labeled as the lower band and the higher band, respectively.

tential varies in the gap. In the metallic region, however, since the occupied states varies with the chemical potential, thus M_c also varies with μ , resulting in a decreasing slope in the lowest three metallic regions and a increasing slope in the highest two metallic regions, as shown in Fig. 4(b). The Berry phase term M_Ω also displays different behavior between insulating and metallic regions. In the lowest two insulating region, M_Ω linearly increases with μ , and in the gap-IV, M_Ω linearly decreases with μ , as is expected from Eq. (3). In the metallic region, however, this term sensitively depends on the topological property of the band in which the chemical potential is located. For the bands with nonzero Chern number, one can see from Fig. 4(b) that M_Ω remains invariant, while for the band 2 (its Chern number is zero), it increases with the chemical potential μ . On the whole the comparison between Figs. 4(a) and 4(b) shows that the metallic behavior of \mathcal{M} is dominated by its conventional term M_c , while in the insulating regime M_Ω plays a main role in determining the behavior of \mathcal{M} . The behavior of the OM in this case is similar to that in the strong spin coupling limit.

Then we study the case II. Similar to the case I, we firstly draw the energy spectrum in Fig. 5(a), from which one can find that there are only two gaps, which can be called the lower and the higher gap, respectively. In this case the gaps between bands 2 and 3, between 3 and 4 (the Mott gap), and between 5 and 6 vanish. We also draw in Fig. 5(b) the corresponding Hall conductivity as a function of the electron Fermi energy.

Figure 6(a) plots the OM (\mathcal{M}) as a function of the electron chemical potential μ . One can see that initially the OM rapidly decreases as the filling of the lower band increases, arriving at a minimum at $\mu=-2.68$, a value corresponding to the top of the lower band. Then, as the chemical potential continues to vary in the lower gap, the OM goes up and increases as a linear function of μ . This linear relationship in the insulating region can also be understood by Eq. (12). Because the gap between 2 and 3 and the Mott gap vanish, the OM displays a more

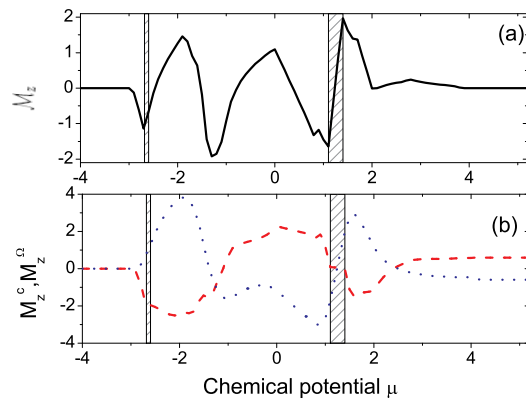


FIG. 6: (Color online) (a) The OM and (b) its two components M_c (dashed line) and M_Ω (dotted line) as a function of the chemical potential μ . The parameters are same as those in Fig. 5.

complex behavior in this metallic region. The value of the OM oscillate versus the chemical potential μ . When μ reaches the bottom of the higher gap, the OM begins to go up again and linearly increases. Different from in the lower gap, the coefficient of the increasing is twice of that in the lower gap, which can be understood by Eq. (12). In the higher gap $d\mathcal{M}/d\mu=-(e/h)\sum_{n=1}^4 C_n=2e/h$, while in the lower gap, $d\mathcal{M}/d\mu=-(e/h)C_1=e/h$.

To see the different roles M_c and M_Ω play in the metallic and insulating regions, we draw in Fig. 6(b) M_c and M_Ω as a function of the chemical potential, their sum gives \mathcal{M} in Fig. 6(a). In each insulating area the conventional term M_c keeps a constant and M_Ω linearly increases with μ in the two gaps with different linear coefficients, as is expected from Eq. (3). The behaviors of OM in this case is novel, comparing with those in the infinite Hund's coupling case. There are two features in the regime $J_0 < J_c$. One is that the magnitudes of both two parts M_c and M_Ω become much smaller than those in the regime $J_0 > J_c$. The other is that in the metallic region, both two parts rapidly changes. The reason is that the gaps between bands 2, 3 and 4 vanish and these bands form one energy band. However from Fig. 6(b) one can see that the two parts of \mathcal{M} have opposite contributions to \mathcal{M} , which implies that these two parts carry opposite-circulating currents.

V. ANOMALOUS NERNST EFFECT

The above discussion of M_c and M_Ω can be transferred to study the ANE. The relation between the OM and ANE has been recently found [12]. To discuss the transport measurement, it is important to discount the contribution from the magnetization current, a point which has attracted much discussion in the past. Motivated by the argument [22] that the magnetization current cannot be measured by conventional transport experiments, Xiao

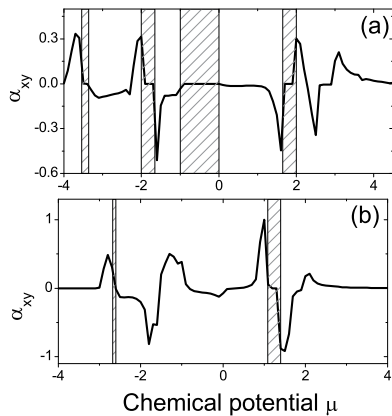


FIG. 7: The ANE of the 2D kagomé lattice at $k_B T=0.005$. The parameters are (a) $\theta=\pi/3$ and $J_0=2$; (b) $\theta=\pi/3$ and $J_0=1$. The shaded areas are the energy gaps.

et al. [12] have built up a remarkable picture that the conventional orbital magnetic moment M_c does not contribute to the transport current, while the Berry phase term in Eq. (2) directly enters and therefore modifies the intrinsic transport Hall current equation as follows

$$\mathbf{j}_H = -\frac{e^2}{\hbar} \mathbf{E} \times \sum_n \int \frac{d^2k}{(2\pi)^2} f_n(\mathbf{r}, \mathbf{k}) \Omega_n(\mathbf{k}) - \nabla \times \mathbf{M}_\Omega(\mathbf{r}), \quad (13)$$

In the case of uniform temperature and chemical potential, obviously, the second term is zero and the Hall effect of 2D kagomé lattice is featured by nonzero Chern number as discussed by Taillefer et al. [9] as well as in this paper. In the following, however, we turn to study another situation, where the current-driving force is not provided by the electric field ($\mathbf{E}=0$). Instead, it is provided by a statistical force, i.e., the gradient of temperature T . In this case, Eqs. (13) and (2) give the expression of intrinsic thermoelectric Hall current as $j_x = \alpha_{xy}(-\nabla_y T)$, where the anomalous Nernst conductivity α_{xy} is given by [12]

$$\alpha_{xy} = \frac{1}{T} \frac{e}{\hbar} \sum_n \int \frac{d^2k}{(2\pi)^2} \Omega_n \times \left[(\epsilon_{n\mathbf{k}} - \mu) f_n + k_B T \ln \left(1 + e^{-\beta(\epsilon_{n\mathbf{k}} - \mu)} \right) \right]. \quad (14)$$

Figure 7 shows α_{xy} of the 2D kagomé lattice as a function of the chemical potential for $k_B T=0.005$. One can see that the ANE disappears in the insulating regions, and when scanning the chemical potential through the bands, there will appear peaks and valleys. Remarkably, a similar peak-valley structure was also found by the recent first-principles calculations in $\text{CuCr}_2\text{Se}_{4-x}\text{Br}_x$ compound [12]. The ANE of this compound was recently measured by Lee et al. [13] as a function of Br doping x which is used to change the chemical potential μ . Due to the scarce data available, until now the peak-valley structure of α_{xy} revealed in Fig. 7 and in Ref. [12, 15, 16] has not been found in experiment, and more direct experimental results are needed for quantitative comparison with the theoretical results. Interestingly, the expression for α_{xy} can be simplified at low temperature as the Mott relation [12],

$$\alpha_{xy} = -\frac{\pi^2}{3} \frac{k_B^2 T}{e} \frac{\partial \sigma_{xy}(\mu_0)}{\partial \mu_0}. \quad (15)$$

Thus one can see that unlike the anomalous Hall effect [23], ANE is given by the Fermi-surface contribution of the band structure and Berry curvature. Another unique feature of α_{xy} is its linear dependence of temperature.

VI. SUMMARY

We have theoretically studied the OM and ANE of the 2D kagomé lattice with spin anisotropies included in a general Hund's coupling region, as a supplement of the previous work [15] in the infinite Hund's coupling limit. The results show that both of the strength of the Hund's coupling and the chirality contribute to the orbital magnetization \mathcal{M} . Upon varying both these parameters, it is found that the two parts of \mathcal{M} , i.e., the conventional part \mathbf{M}_c and the Berry-phase correction part \mathbf{M}_Ω , oppose each other. We also calculate the anomalous Nernst conductivity and obtain a peak-valley structure as a function of the electron Fermi energy.

Acknowledgments

This work was supported by NSFC under Grants Nos. 10604010 and 10544004.

-
- [1] S.T. Bramwell and M.J.P. Gingras, *Science* **294**, 1495 (2001).
 [2] A.P. Ramirez, *Annu. Rev. Mater. Sci.* **24**, 453 (1994); M.J. Harris and M.P. Zinkin, *Mod. Phys. Lett. B* **10**, 417 (1996).
 [3] M.J. Harris, S.T. Bramwell, D.F. McMorrow, T. Zeiske,

- and K.W. Godfrey, *Phys. Rev. Lett.* **79**, 2554 (1997); S.T. Bramwell and M.J. Harris, *J. Phys.: Condens. Matter* **10**, L215 (1998); R. Moessner, *Phys. Rev. B* **57**, R5587 (1998).
 [4] V. Kalmeyer and R.B. Laughlin, *Phys. Rev. Lett.* **59**, 2095 (1987); G. Baskaran and P.W. Anderson, *Phys.*

- Rev. B **37**, 580 (1988); R.B. Laughlin, Science **242**, 525 (1988); X.G. Wen, F. Wilczek, and A. Zee, Phys. Rev. B **39**, 11413 (1989); P.A. Lee and N. Nagaosa, Phys. Rev. B **46**, 5621 (1992); K. Yang, L.K. Warman, and S.M. Girvin, Phys. Rev. Lett. **70**, 2641 (1993).
- [5] Y. Taguchi and Y. Tokura, Phys. Rev. B **60**, 10280 (1999).
- [6] T. Katsufuji, H.Y. Hwang, and S.-W. Cheong, Phys. Rev. Lett. **84**, 1998 (2000).
- [7] K. Ohgushi, S. Murakami, and N. Nagaosa, Phys. Rev. B **62**, R6065 (2000).
- [8] Y. Taguchi and Y. Tokura, Europhys. Lett. **54**, 401 (2001); Y. Taguchi, T. Sasaki, S. Awaji, Y. Iwasa, T. Tayama, T. Sakakibara, S. Iguchi, T. Ito, and Y. Tokura, Phys. Rev. Lett. **90**, 257202 (2003); Y. Yasui, S. Iikubo, H. Harashina, T. Kageyama, M. Ito, M. Sato, and K. Kakurai, J. Phys. Soc. Jpn. **72**, 865 (2003).
- [9] M. Taillefumier, B. Canals, C. Lacroix, V.K. Dugaev, and P. Bruno, Phys. Rev. B **74**, 085105 (2006).
- [10] D. Xiao, J. Shi, and Q. Niu, Phys. Rev. Lett. **95**, 137204 (2005).
- [11] T. Thonhauser, D. Ceresoli, D. Vanderbilt, and R. Resta, Phys. Rev. Lett. **95**, 137205 (2005).
- [12] D. Xiao, Y. Yao, Z. Fang, and Q. Niu, Phys. Rev. Lett. **97**, 026603 (2006).
- [13] W.-L. Lee, S. Watauchi, V.L. Miller, R.J. Cava, and N.P. Ong, Science **303**, 1647 (2004); Phys. Rev. Lett. **93**, 226601 (2006).
- [14] D. Ceresoli, T. Thonhauser, D. Vanderbilt, and R. Resta, Phys. Rev. B **74**, 024408 (2006).
- [15] Z. Wang and P. Zhang, Phys. Rev. B **76**, 064406 (2007).
- [16] Z. Wang, P. Zhang, and J. Shi, Phys. Rev. B **76**, 094406 (2007).
- [17] M.-C. Chang and Q. Niu, Phys. Rev. B **53**, 7010 (1996).
- [18] G. Sundaram and Q. Niu, Phys. Rev. B **59**, 14915 (1999).
- [19] Z. Wang, and P. Zhang, cond-mat/0711.2725v1, to appear in Phys. Rev. B.
- [20] D.J. Thouless, *Topological Quantum Numbers in Nonrelativistic Physics* (World Scientific, Singapore, 1998).
- [21] Z. Wang and P. Zhang, unpublished.
- [22] N.R. Cooper, B.I. Halperin, and I.M. Ruzin, Phys. Rev. B **55**, 2344 (1997).
- [23] F.D.M. Haldane, Phys. Rev. Lett. **93**, 206602 (2004).